Mass spectral characterization of secondary organic aerosol from urban cooking and vehicular sources ~~emissions~~

Wenfei Zhu[1], Song Guo[1,2*], Min Hu[1], Zirui Zhang[1], Hui Wang[1], Ying Yu[1], Zheng Chen[1], Ruizhe Shen[1], Rui Tan[1], Kai Song[1], Kefan Liu[1], Rongzhi Tang[1], Yi Liu[1], Shengrong Lou[3], Yuanju Li[1], Wenbin Zhang[4], Zhou Zhang[4], Shijin Shuai[4], Hongming Xu[4], Shuangde Li[5], Yunfa Chen[5], Francesco Canonaco[6], Andre. S. H. Prévôt[6]

[1] *State Key Joint Laboratory of Environmental Simulation and Pollution Control, International Joint Laboratory for Regional Pollution Control, Ministry of Education (IJRC), College of Environmental Sciences and Engineering, Peking University, Beijing 100871, China P. R.*
[2] *Collaborative Innovation Center of Atmospheric Environment and Equipment Technology, Nanjing University of Information Science & Technology, Nanjing 210044, China P. R.*
[3] *State Environmental Protection Key Laboratory of Formation of Urban Air Pollution Complex, Shanghai Academy of Environmental Sciences, Shanghai 200233, China P. R.*
[4] *State Key Laboratory of Automotive Safety and Energy, Tsinghua University, Beijing 100084, China P. R.*
[5] *State Key Laboratory of Multiphase Complex Systems, Institute of Process Engineering, Chinese Academy of Sciences, Beijing 100190, China P. R.*
[6] *Laboratory of Atmospheric Chemistry, Paul Scherrer Institute (PSI), Villigen 5232, Switzerland*

Corresponding authors:

*Song Guo − State Key Joint Laboratory of Environmental Simulation and Pollution Control, College of Environmental Sciences and Engineering, Peking University, Beijing 100871, China P. R.; Email: songguo@pku.edu.cn

Abstract In the present work, we conducted experiments of secondary organic aerosol (SOA) formation from urban cooking and vehicular sources to characterize the mass spectral features of primary organic aerosol (POA) and SOA using an high-resolution time-of-flight aerosol mass spectrometer (HR-ToF-AMS). Our results showed that the cooking styles have a greater impact on aged COA mass spectra than oxidation conditions. However, the oxidation conditions affect the aged HOA spectra more significantly than vehicle operating conditions. In our study, we use mass spectra similarity analysis and positive matrix factorization (PMF) analysis to establish the POA and SOA mass spectra of these two sources. These mass spectra are used

as source constraints in a multilinear engine (ME-2) model to apportion the OA sources in the atmosphere. Comparing with the traditional ambient PMF results, the improved ME-2 model can better quantify the contribution of POA and SOA from cooking and vehicular sources. Our work, for the first time, establishes the vehicle and cooking SOA source profiles, and can be further used in the OA source apportionment in the ambient atmosphere.
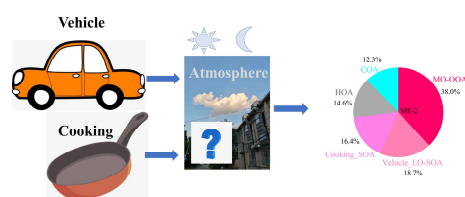
1. Introduction

Organic aerosol (OA) is an important component of fine particulate matter and has significant environmental and health effects, especially in urban areas (Guo et al., 2012; Guo et al., 2014; Ying et al., 2020). Currently, real-time measurements of OA based on the aerosol mass spectrometer (AMS) has become an effective way to explore OA characteristics in the field campaigns and laboratory studies (Canagaratna et al., 2007; Ge et al., 2017; Hu et al., 2016a; Huang et al., 2011; Kim et al., 2017; Li et al., 2017; Sun et al., 2016; Zhang et al., 2011). Applying positive matrix factorization (PMF) and a multilinear engine (ME-2) (Paatero, 1999) to analyze the high-resolution mass spectrometry fragments, OA can be further identified as primary organic aerosol (POA) and secondary organic aerosol (SOA). POA includes a kind of hydrocarbon-like OA, (HOA), cooking (COA), and biomass burning (BBOA), which SOA includes low oxygenated OA (LO-OOA) and more oxygenated OA (MO-OOA)(Canonaco et al., 2013; Elser et al., 2016; Qin et al., 2017; Zhang et al., 2017a; Zhou et al., 2018). Many previous studies have been found that HOA is mainly associated with vehicle-related emissions in the urban atmosphere (Hu et al., 2017; Xu et al., 2016; Zhang et al., 2017a). Hereinafter, HOA will be referred to as the abbreviation for organic aerosol emitted by urban vehicles. As lifestyle sources in urban, cooking and vehicular sources ele emissions, that is COA and HOA mostly determine

ambient OA loadings. For example, primary cooking OA (COA) and vehicle exhaust OA (HOA) accounted for 10-35 % and 6-26% of OA, respectively, in urban areas in China (He et al., 2011; Hu et al., 2017; Sun et al., 2010; Sun et al., 2014; Sun et al., 2018; Wang et al., 2016; Xu et al., 2016; Zhang et al., 2014).

Besides the contribution to POA, many studies have found that cooking and vehicular sources may also emit a large number of volatile organic compounds (VOCs) (Gentner et al., 2009; Katragadda et al., 2010; Klein et al., 2016), semi-volatile organic compounds (SVOCs), and intermediate volatile organic compounds (IVOCs) ($\geq$C13n-alkanes and fatty acids) (Louvaris et al., 2017; Schauer et al., 2002; Tang et al., 2021), which may also play important roles in SOA formation(Wang et al., 2021; Yu et al., 2021). However, based on collocated AMS measurements and factor analysis results, the SOA formed by vehicle and cooking sources cannot be effectively resolved from the total SOA due to the lack of secondary mass spectral profiles. The POA mass spectral profiles based on AMS including HOA (Collier et al., 2015), BBOA (Alfarra et al., 2007; He et al., 2010; Xu et al., 2020), and COA (He et al., 2010; Liu et al., 2017; Mohr et al., 2012; Xu et al., 2020) have been fully explored in laboratory studies and applied as constraint factors into the ME-2 model in the ambient air. Some studies have made it possible to quantify biogenic secondary aerosol products of a single precursor, such as isoprene oxidation products (IEPOX) (Budisulistiorini et al., 2013; Hu et al., 2016b), and have been extended to the urban atmosphere to obtain an IEPOX-SOA factor via PMF analysis of OA spectra (Zhang et al., 2017b). Although several studies explored the mass spectral characteristics of SOA from cooking and vehicular sources, i.e., heated cooking oils, gasoline motors, and diesel engines (Kaltsonoudis et al., 2017; Kroll et al., 2012; Liu et al., 2018; Presto et al., 2014), the spectral profiles of cooking SOA under actual cooking conditions and vehicle SOA under different emission conditions are still uncertain. Besides, to date, studies that used ME-2 for a better anthropogenic SOA source apportionment by inputting their SOA spectra as constraints remain scarce. Therefore, the mass spectra of SOA from abundant cooking and vehicular sources are urgent to characterize for conducting to acquire a better source apportionment of SOA.

In this study, cooking and vehicle experiments were carried out to investigate the variation in POA and SOA spectra profiles emitted from vehicle emissions under different running conditions, and Chinese cooking emissions under different cooking styles using high-resolution time-of-flight AMS (HR-ToF-AMS). The mass spectral characterizations of POA and SOA from cooking and vehicle emissions were intercompared, and their changes in some indicated ionic fragments were elucidated. Besides, we verified the mass spectral profiles by applying POA and SOA profiles to ME-2 for source apportionment of OA in the winter observation with various primary emissions and the summer observation with high oxidation conditions.

2. Materials and Methods

2.1 Simulation of POA emission and SOA formation from cooking and vehicular sources.

For cooking, we prepared four dishes including deep-frying chicken, shallow-frying tofu, stir-frying cabbage, and Kung Pao chicken. The total cooking time for each experiment ranged from 40 to 66 min, which was almost related to the features of each dish (**Table S1**). Each dish was continuously carried out 8 times in parallel during the cooking process until the closed kitchen was full of fumes. The fumes produced by cooking were introduced through the pipeline from the kitchen into the Gothenburg Potential Aerosol Mass (Go: PAM) reactor (Li et al., 2019) in the laboratory after being diluted 8 times by a Dekati Dilutor (e-Diluter, Dekati Ltd., Finland). Heat insulation cotton was wrapped around the sampling pipelines to prevent fumes from condensing on the wall of the pipe. We considered the emissions sampled after Go: PAM without OH radical as primary emissions, and those monitoring after Go: PAM with given OH radicals as secondary formation. The sampling time ranged from 58 to 90 min. ~~Each sampling was in parallel three times. The relative standard deviations were small, which were under 10% in most cases.~~ In addition, the background blank groups and the dilution gas blank groups were separately completed using boiling water and dilution gas, according to the same steps as experimental groups. More information on the experimental setup of cooking simulations has been given in (Zhang et al., 2020).

97   For vehicle, experiments were performed by using a Gasoline direct engine (GDI)with a commercial

98   China V gasoline fuel (Emission: 998cc; Maximum power: 100KW 6000rpm; Peak torque: 205Nm 2000-

99   3000rpm). Vehicle operating under real-life conditions were dynamic rotating speed-torque combination. For

100   example, the combination of 1500 rpm rotating speed and 16Nm torque, and 2000rpm, rotating speed and

101   16Nm torque for the engine in this study reflect the realistic vehicle speed of 20km/h and 40km/h, respectively.

102   Five running conditions covering different speeds and torques, including 1500rpm_16Nm, 1750rpm_16Nm,

103   2000rpm_16Nm, 2000rpm_32Nm, and 2000rpm_40Nm, were used to characterize their POA and SOA mass

104   spectra in this study. Once the engine warmed up, it continued to work under one running condition. After the

105   three-way catalytic system, the exhaust from the engine tailpipe was diluted 30 times by the same dilution

106   system for the cooking experiment. Then the diluted exhaust entered the GO: PAM through the stainless pipe

107   wrapped by heat insulation cotton. For each running condition, five parallel experiments were conducted

108   (**Table S2**). The sampling time with collecting three parallel data groups was about 60 min for each experiment.

109   Go: PAM reactor consists of quartz tube that is 100 cm long and 9.6 cm in diameter, as described in

110   (Watne et al., 2018). The OH radicals in Go: PAM reactor is generated by the photolysis of ozone and the

111   reaction in the presence of water vapor. We adjusted input ozone concentrations ranging from ~0 to ~6.5 ppm

112   and ~0 to ~4.0 ppm to change the OH radicals in the Go: PAM for vehicle and cooking experiments,

113   respectively. The temperature, relative humidity, and the sampling residence time in Go: PAM for vehicle and

114   cooking experiments were documented in the supplement material (**Table S3**).

115 **2.2 Instrumentation and data analysis.**

116   The design drawing on vehicle and cooking experiments is presented in **Figure S1**. Two scanning

117   mobility particle sizers (SMPS; TSI Incorporation, USA) were set at the inlet and outlet of Go: PAM to correct

118   the wall loss (Zhang et al., 2020). The size distribution and number concentration of particles were scanned

119   every 2 (cooking) - 5 min (vehicle) before and after Go: PAM for cooking and vehicle experiment, respectively.

The mass concentrations of non-refractory submicron aerosol (NR-PM$_1$), and high-resolution ions fragments

of OA were recorded by HR-ToF-AMS (Aerodyne Research Incorporation, USA), synchronize with SMPS.

Before and after the two experiments, the ionization efficiency (IE) of HR-ToF-AMS was calibrated by

applying 300 nm mono-dispersed ammonium nitrate particles synchronization with SMPS. The collection

efficiency (CE) was obtained from comparing AMS and synchronous SMPS real-time measurement of particle

mass concentrations at the outlet of Go: PAM. Besides, the real-time measurements of CO_2 concentrations

(Model 410i, Thermo Electron Corporation, USA) were used to correct the influence of CO_2 on OA ion

fragments, refer to (Canagaratna et al., 2015). Other gas phase measurements included carbon monoxide (CO,

Thermo, Model 48i TL), NO$_x$ (Thermo, Model 42i TL), and SO$_2$ (Thermo, Model 42i TL).

The mass concentration, size distribution, and the ion-speciated mass spectra of NR-PM$_1$ species were

analyzed using the HR-ToF-AMS standard data analysis software (SQUIRREL version 1.57 and PIKA version

1.16). The elemental compositions (O/C, H/C, N/C, and OM/OC) were estimated by the "improved-ambient"

updated method (Canagaratna et al., 2015). The OH exposure and equivalent photochemical age (EPA) were

calculated by off-line methods according to SO$_2$ decay shown in (Zhang et al., 2020), which were validated

by a flow reactor exposure estimator using measured concentrations of reactive compounds such as VOCs,

CO, and NO$_x$ (Peng et al., 2016). The OH exposure and photochemical age for all conditions in cooking and

vehicle experiments were listed in **Table S3**.

2.3 OA source apportionment

The PMF model can describe the variability of a multivariate database as a linear combination of static

factor profiles and their corresponding time series (Huang et al., 2020; Wang et al., 2017; Zhu et al., 2018). In

this study, we used the Igor-based PMF model with PMF2.exe algorithm (Paatero and Hopke, 2003) and the

PMF Evaluation Toolkit version 2.08D (Ulbrich et al., 2009) to split POA and SOA factors from cooking and

vehicle aged OA. The PMF model was also used to identify the source of OA for ambient atmosphere during

143 the summer and winter observations of Shanghai, following the procedure presented in the literature (Hu et

144 al., 2016a; Zhang et al., 2011), as described in section 3.3. In contrast to an unconstrained PMF analysis, ME-

145 2 algorithm allows the user to add prior information (e.g., source profiles) into the model to constrain the

146 matrix rotation and separated the mixed solution. In this study, we adopted the toolkit SoFi (Source Finder)

147 with an ~~in~~ a-value approach to perform organic HR-AMS datasets collected in Shanghai. The a-value can vary

148 between 0 and 1, which is the extent to which the output profiles can vary from the model inputs. The a-value

149 test was performed following the technical guidelines presented in ~~(~~Crippa et al., 2014~~)~~. The reference mass

150 spectral profiles that constrained in ME-2 analysis were derived from lab-based primary and secondary

151 cooking and vehicular factors of this study. Details of the algorithm could refer to previous studies (Canonaco

152 et al., 2013; Huang et al., 2020; Reyes-Villegas et al., 2016).

153 **2.4 Mass spectra similarity analysis.**

154   In this study, the angle θ was used to evaluate the correlation between the two AMS mass spectra features.

155 The angle θ between the two AMS mass spectra (MSa, MSb) is given by:

$$\cos\theta = \frac{MSaMSb}{|MSa||MSb|}$$

157   The θ angle between two mass spectra is 0-5, 5-10, 10-15, 15-30, and > 30, which means excellent

158 consistency, good consistency, many similarities, limited similarities, and poor consistency, respectively~~,~~

159 (Kaltsonoudis et al., 2017; Kostenidou et al., 2009).

160 **3.   Results and Discussion**

161 **3.1 Mass spectra of POA and aged OA from the cooking and vehicular sources.**

162   **Fig.1a** shows the mass spectra of aged HOA under different vehicle running conditions when EPA was

163 0.6 days. The mass spectra of aged HOA emission from different vehicle running conditions under other

164 various oxidation degrees are included in **Fig.S2**. All the aged HOA spectral profiles from different vehicle

165 running conditions showed a similar pattern, and the θ angles among the mass spectra of aged HOA were less

than 10° at EPA 0.6 days (**Table 1**), suggesting a little difference between the mass spectra. The mass spectra

of aged HOA at 0.6 days were dominated by the ion series of $C_nH^+_{2n+1}$ (m/z 29, 43, 57, 71, 85...) and $C_nH_{2n-1}^+$

(m/z 41, 55, 69, 83...), resulting from less oxidized components such as saturated alkanes, alkenes. As the

highest proportion of ion fragments, m/z 43 and 29 consisted of oxygen-containing ions like CHO^+ and

$C_2H_3O^+$, respectively, whose fractions were much larger than the hydrocarbon-like ion fragments at the same

mass integers. Besides, there were also abundant tracer ion fragments for SOA (m/z 28 and m/z 44).

(a) Aged HOA at EPA 0.6 day	(b) Aged COA at EPA 0.7 day
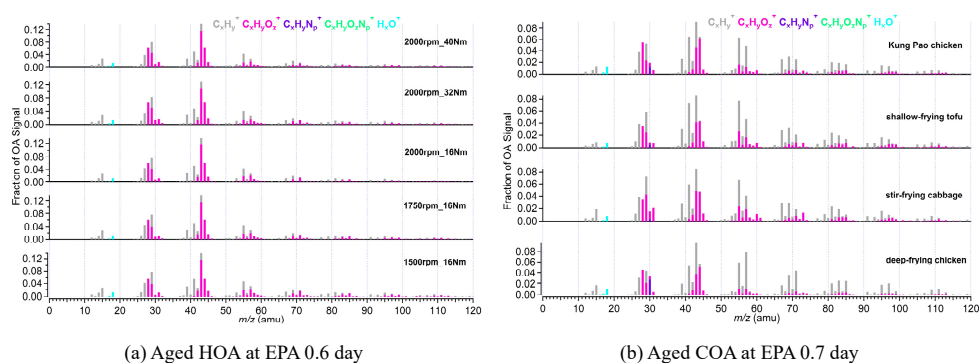
Fig.1. (a) The mass spectra of aged HOA emission from different vehicle running conditions at EPA 0.6 day; (b) The mass spectra of aged COA from four Chinese dishes at EPA 0.7 day. Five running conditions cover different speeds and torques, including 1500rpm_16Nm, 1750rpm_16Nm, 2000rpm_16Nm, 2000rpm_32Nm, and 2000rpm_40Nm. Four dishes include deep-frying chicken, shallow-frying tofu, stir-frying cabbage, and Kung Pao chicken.

The mass spectra of aged COA at 0.7 days of EPA are presented in **Fig.1b**. Detailed mass spectra of aged

COA under other various oxidation degrees are included in **Fig.S3**. The similarity of aged COA among

different types of cooking was greater than that of aged HOA among different running conditions when the

EPA was at the same level. Except for the θ angles of deep-frying chicken vs stir-frying cabbage (21°), and

deep-frying chicken vs shallow-frying tofu (19°), the θ angles among other aged COA at EPA 0.7 day exhibited

good agreement (θ<15°) in mass spectra (**Table 1**). The mass spectra of cooking were dominated by the similar

ion series as those of vehicle, which were mostly m/z 28, m/z 29, m/z 41, m/z 43, m/z 44, m/z 55, m/z 57, m/z

67, and m/z 69. However, the major mass spectral differences between cooking and vehicle were the abundance of m/z 41 and the ratio of oxygen-containing ions to hydrocarbon ions ($C_xH_yO_z^+/C_xH_y^+$). The four Chinese dishes had prominent peaks at m/z 41, m/z 43, and m/z 55 (generated from $C_3H_5^+$ and $C_3H_7^+$, $C_4H_7^+$) which was qualitatively consistent with mass spectra of primary COA in other studies (Xu et al., 2020). As described by (He et al., 2010), the most abundant ion fragments at m/z 41 and m/z 55 from primary Chinese cooking emissions associated with frying are resulting from unsaturated fatty acids

Table 1 The θ angles among the mass spectra of (a) aged HOA at EPA 0.6 day and (b) aged COA at EPA 0.7 day

(a) θ angles	1500rpm_16Nm	1750rpm_16Nm	2000rpm_16Nm	2000rpm_32Nm	2000rpm_40Nm
1500rpm_16Nm	0	3	3	8	4
1750 rpm_16 Nm		0	0.1	5	3
2000 rpm_16 Nm			0	5	3
2000 rpm_32 Nm				0	4
2000 rpm_42 40 Nm					0

(b) θ angles	deep-frying chicken	stir-frying cabbage	shallow-frying tofu	Kung Pao chicken
deep-frying chicken	0	21	19	14
stir-frying cabbage		0	10	13
shallow-frying tofu			0	12
Kung Pao chicken				0

Fig.2a shows the mass spectra of aged HOA oxidation at different OH exposures under the same vehicle running condition (2000rpm, 16Nm). The changes in mass spectra of aged HOA under different conditions are provided in **Fig.S4**. It was worth noting that the source characteristics of vehicle POA were uncertain due to its low concentration emitted from the engine in this study **(Table S4)**. A related study has found that the POA factor from vehicle emissions is similar to the HOA factor derived from environmental datasets (Presto et al., 2014). Therefore, we used the average HOA spectrum derived from unconstrained PMF analysis based

on the ambient observations of Shanghai, Beijing, Dezhou, Shenzhen in China as an alternative to the mass

spectrum of vehicle POA, as shown in **Fig.2a** and **Fig.S4**. Detail observation information of Shanghai, Dezhou,

and Shenzhen referred to (Zhu et al., 2021a). The observations in Beijing have been given in (Hu et al., 2017).

The HOA spectrum was similar to that reported in (Ng et al., 2011), which has been widely used as traffic

emission profiles. As the oxidation degree increased, the ion fragments varied similarly with hydrocarbon-like

ion fragments decreasing. The mass spectra at 2.9 days and 4.1 days had very similar patterns with the most

abundant signals at m/z 28 and 44, respectively (**Fig.2** and **Fig.S4**), which showed good consistency with the

mass spectra of MO-OOA resolved from ambient datasets(θ = 14°; compared with MO-OOA obtained during

the spring observations in (Ng et al., 2011; Zhu et al., 2021b). When EPA was 1.7 days, there were different

mass spectra patterns, with dominant signals at m/z 28 and m/z 44, yet contained a large signal at m/z 43,

many similarities with the spectra of the ambient LO-OOA (**Fig.2** and **Fig.S4**) (Hu et al., 2017; Zhu et al.,

2021b). Oxidation degrees greatly affected the similarity of mass spectra between POA and those of aged

HOA. The mass spectra profile of HOA_ambient displayed poor agreement (θ > 30°) with all aged HOA

spectra profiles (**Tables** ~~S6~~**S7**). Besides, the mass spectra under the low oxidation degree (EPA was 0.6 day)

was also poorly correlated with those mass spectra under the high oxidation degree (EPA were 2. 9 and 4.1

days) (**Table** ~~S6~~**S7**).
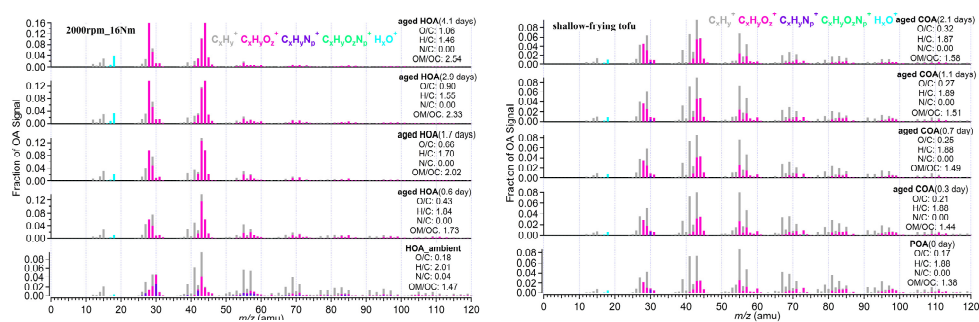
Fig.2. (a) The mass spectra of HOA and aged HOA oxidation under four different OH exposure at the same running

condition (2000rpm, 16Nm). (b) The mass spectra of primary COA and aged COA oxidation of different OH exposure for shallow-frying tofu. The EPA was obtained from off-line methods according to SO_2 decay shown in Table S3. The elemental compositions were estimated by the "improved-ambient" updated method (Canagaratna et al., 2015).

214

215   The mass spectra of primary COA and aged COA showed great inter-correlations ($\theta < 15°$), which were

216   smaller than that of vehicle OA (**Table S7S8**). The spectra of aged COA derived herein displayed good

217   consistency with those from cooking oils (Liu et al., 2018) (**Fig.2b** and **Fig.S5**). It should be noted that the

218   fractions of m/z 28 and m/z 44 signals in aged COA were lower than those of aged HOA at the similar EPA.

219   In addition, the aged COA had more hydrocarbon-like ions at the same mass integers than aged HOA.

220   All the above results imply that oxidation condition drives the variabilities in mass spectra of the vehicle

221   OA. In contrast, cooking styles instead of oxidation conditions significantly affected the mass spectra of

222   cooking OA. Here we concluded some possible explanations for these results. On one hand, under the same

223   oxidation conditions and different emission conditions, the similarity among the mass spectra of vehicles was

224   larger than that of cooking, which may be related to their precursors. Some studies have shown that the species

225   and the proportion of gaseous organic matter emitted by different dishes are quite different (Wang et al., 2018).

226   As described in the literature, alkanes and oxygenated volatile organic compounds (O-VOCs) contributed to

227   over 97% of the total VOCs for fried food, and O-VOCs were the dominant contributors for Sichuan and

228   Hunan cuisine where stir-frying is common (Wang et al., 2018). Different gaseous precursors cause

229   distinctions in the particle phase SOA formation, which is reflected in the variations of AMS ion fragments

230   between four dishes in our study. Compared to cooking, the precursors from vehicles are mainly hydrocarbons,

231   and the difference in emissions under different running conditions is inapparent (Robinson et al., 2007). On

232   the other hand, under the same emission conditions and different oxidation conditions, the similarity among

233   the mass spectra of cooking sources is larger than that of vehicle sources, likely due to the oxidation pathway

234   of precursors. As mentioned above, O-VOCs are important precursors of cooking sources, and their oxidation

235   mechanisms are mostly alcohol/peroxide substitution process. This conclusion was proved by a Van Krevelen

236 diagram, showing that the cooking data gather around the slope of approximately -0.1 (Zhang et al., 2020), in

237 agreement with that of heated oils OA (Liu et al., 2018). However, for vehicles, with the increase of oxidation

238 degrees, the reaction pathways of hydrocarbon precursors varied diversely. In Van Krevelen space, the vehicle

239 data fell along a line with a slope of -0.5 (**Fig.S6**), indicating oxidation processes involving the addition of

240 both carboxylic acid and alcohol or peroxide functional groups without fragmentation and/or the addition of

241 carboxylic acid functional groups with fragmentation.

242 **3.2 Identification of the cooking and vehicular sources SOA mass spectra.**

243 Although the f44 (proportion of m/z 44 in OA) of aged COA raised from 0.03 to 0.08 with oxidation

244 increasing (**Fig.2b** and **Fig.S5**), the high abundance of m/z 41, 55, and 57 in aged COA mass spectra for four

245 dishes may be a sign that aged COA identified in this study is a mixture of POA and SOA. PMF analysis was

246 performed on the high-resolution mass spectra to split SOA and POA factors from integrated primary COA

247 and aged COA under each dish. Similarly, the same PMF procedure was also applied for vehicle aged datasets

248 for each running condition. The choice of the PMF solution can be found in the supplement material (**Fig.S7-**

249 **S10** and **Table** S8S9-S9S10; taken stir-frying cabbage for cooking, and 2000rpm_32Nm for vehicle as an

250 example).

251 Some ions like m/z 41, 55, 57, 43, 28, and 44 are typically used as tracers of OOA, COA, HOA, LO-

252 OOA, and MO-OOA. **Fig.3** shows the high-resolution mass spectra of POA and SOA from four Chinese dishes

253 and five vehicle running conditions. The cooking PMF POA of four Chinese dishes all showed obvious

254 hydrocarbon-like signals at m/z 41, 43, 55, and 57, 67, and 69 with ion fragments of $C_3H_5^+$, $C_3H_7^+$, $C_4H_7^+$,

255 $C_4H_9^+$, $C_5H_7^+$, and $C_5H_9^+$, respectively. The fraction of m/z 41 in cooking POA ranged from 0.051 to 0.069

256 The prominent fraction of m/z 43 (f_{43}=0.068~0.083), 55 (f_{55}=0.064~0.084), 57 (f_{57}=0.041~0.097), 67

257 (f_{67}=0.021~0.40), 69 (f_{69}=0.034~0.049) were observed (Table S10). For mass spectra of cooking PMF SOA,

258 the oxygen oxidationoxidized ion fragments had higher signals than those of hydrocarbon-like ion fragments.

259 The dominate signals existed at m/z 28 (f_{28}=0.045~0.068), 29 (f_{29}=0.048~0.080), 41 (f_{41}=0.050~0.068), 43

260 (f_{43}=0.087~0.103), 44 (f_{44}=0.058~0.080), 55 (f_{55}=0.050~0.064) (Table S11).

261 Different from the cooking, two-vehicle PMF SOA factors were derived from aged HOA, rather than

262 integrated primary HOA and aged HOA datasets due to the low primary HOA emission (**Table S4**), as

263 described in sect. 3.1due to higher OH exposure. Unfortunately, vehicle PMF POA factor cannot be separated

264 from aged HOA due to higher OH exposure. According to different O/C ratios, they were considered to be

265 low oxidized vehicle SOA (LO-SOA) and more oxidized vehicle SOA (MO-SOA). As indicated in **Fig.3** and

266 **Table S12S13**, the prominent m/z 28 (average f_{28}=0.045), 41 (average f_{41}=0.046), 43 (average f_{43}=0.158),44

267 (average f_{44}=0.054), 55 (average f_{55}=0.039), 57 (average f_{57}=0.027) of vehicle PMF LO-SOA were

268 comparable with those of cooking PMF SOA. The fraction of m/z 43 of vehicle PMF LO-SOA was higher

269 than that in cooking SOA by a factor of 2, which may be caused by the inability to separate vehicle PMF POA

270 factor in the PMF analysis. The abundant m/z 28 and 44 (mainly generated from CO_2^+) are widely used as the

271 ambient MO-OOA markers. (Sun et al., 2018; Xu et al., 2017). We observed high factions of m/z 28

272 (f_{28}=0.110~0.214) and m/z 44 (f_{44}=0.121~0.224) in vehicle PMF MO-SOA (Table S13) and high O/C ratios

273 (0.88~1.33), which were much higher than those of vehicle PMF LO-SOA (O/C=0.37~0.53) and cooking SOA

274 (O/C=0.29~0.41).

275

(a) Cooking PMF POA   (b) Cooking PMF SOA

(c) Vehicle PMF LO-SOA   (d) Vehicle PMF MO-SOA
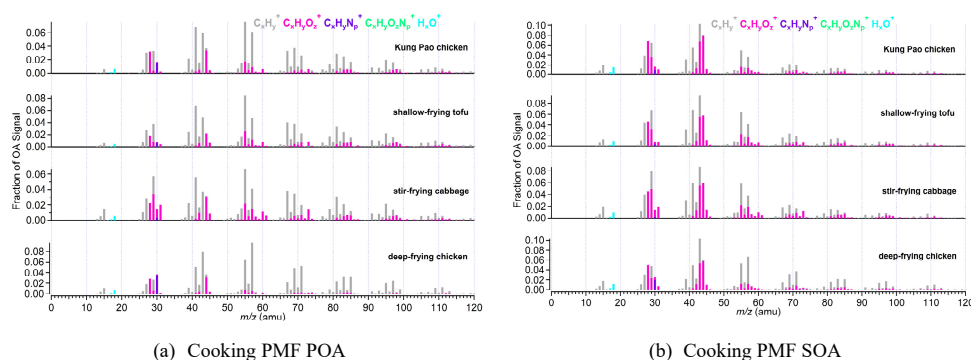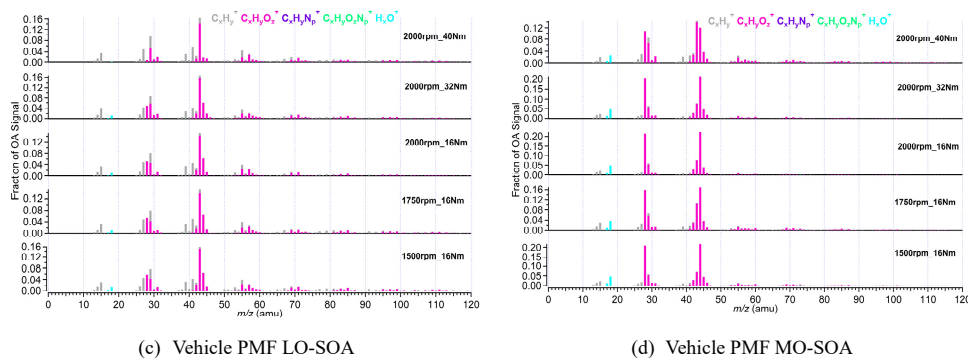
Fig.3. The mass spectra of PMF POA and SOA from vehicle and cooking. PMF analysis was performed on the high-resolution mass spectra to split two factors (cooking POA and SOA) from aged COA and two SOA factors (vehicle LO-SOA and MO-SOA) from aged HOA, respectively.

276

Similarly, for the resolved SOA factors, the correlation of mass spectra among cooking groups under different cooking methods ($\theta = 8\sim21°$) was worse than that of vehicle groups (vehicle PMF LO-SOA; $\theta = 3\sim19°$) under different running conditions (**Table** ~~S14~~ **S15** and **Table** ~~S16~~**S17**). The mass spectra of the PMF POA factors for deep-frying chicken exhibited poor agreement with those of stir-frying cabbage, Kung Pao chicken, and shallow-frying tofu (**Table** ~~S15~~**S16**). In addition, we also found that the θ angles between vehicle PMF LO-SOA and vehicle PMF MO-SOA under five GDI running conditions were ranged from 36° to 50° (**Fig.S11**), indicating that the mass spectra profiles of vehicle PMF LO-SOA are poor consistency with those of vehicle PMF MO-SOA, consistent with the changes in the mass spectra characteristics of vehicles, under the same emission conditions and different oxidation conditions. Our results suggest that it is necessary to consider the cooking styles when constraining cooking and atmospheric oxidation conditions when constraining vehicle factors.

3.3 Application of established POA and SOA profile in ambient OA source apportionment.

The POA and SOA of the cooking as the primary and secondary spectrum constraints for ME-2 were obtained by averaging the high-resolution mass spectra datasets of the four dishes, which were identified from

aged COA using the PMF model. Similarly, combining different GDI running conditions, the averaged vehicle

LO-SOA and vehicle MO-SOA which were resolved based on aged HOA by using the PMF model were used

as the inputting mass spectra profiles of vehicles for ME-2. The mass spectral profiles for cooking and vehicle

as constraints in the ME-2 model are shown in **Fig.S12**.

The θ angles between the mass spectral profiles from urban cooking and vehicular sources and ambient

PMF-resolved factors were calculated and summarized in **Fig.4** and **Table ~~S18~~S19**. The AMS mass spectra of

ambient factors were obtained and averaged in Shanghai, Dezhou, Beijing, and Shenzhen in China (Hu et al.,

2017; Zhu et al., 2021a). The θ angles among ambient COA, HOA, LO-OOA, and MO-OOA factors and the

cooking POA, SOA, and the vehicle LO-SOA, vehicle MO-SOA were ranged from 18° to 52° (**Fig.4**),

suggesting that the cooking POA, cooking SOA, and the vehicle LO-SOA, vehicle MO-SOA can be used as

source constraints for ME-2 in ambient air.
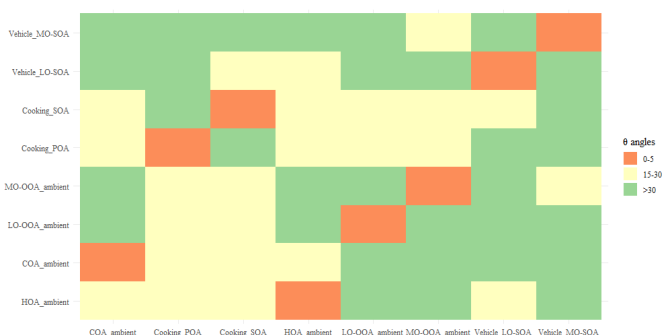
Fig.4. The θ angles between ambient COA, HOA, LO-OOA, and MO-OOA factors and the cooking PMF POA, SOA, and the vehicle LO-SOA, MO-SOA. The θ angle between two mass spectra is 0-5, 5-10, 10-15, 15-30, and > 30 indicates excellent consistency, good consistency, many similarities, limited similarities, and poor consistency, respectively. The ambient COA, HOA, LO-OOA, and MO-OOA factors were averaged the resolved factors which performed on Shanghai, Dezhou, Beijing, and Shenzhen datasets (Hu et al., 2017; Zhu et al., 2021a).

~~Constraining many SOA factors could be over-constraining the ME-2 runs, which leads to factor mixing~~

~~and reduces the number of factors. In addition, considering~~ Considering the actual oxidation conditions, that

is the concentration of OH radicals, and the lacking vehicle POA due to its low emission (**Table S4**), and the

设置了格式: 字体: 加粗

SOA spectra constraining reasonably, the cooking POA, cooking SOA, vehicle LO-SOA, and ambient HOA (instead of vehicle POA; derived from Beijing, Shenzhen, Dezhou, Shanghai ambient measurements) was finally selected as the input source spectra of ME-2. We further demonstrated the feasibility of input primary and secondary mass spectra for OA source apportionment in two field campaigns at the urban site of Shanghai in summer and winter. The ambient measurements in Shanghai were taken in situ at the same location as (Zhu et al., 2021a), i.e., Shanghai Academy of Environmental Sciences (31.10°N,121.25°E), a typical urban site in the Yangtze River Delta region from 23 August to 5 September 2016, and from 28 November 2016 to 12 December 2017 with HR-ToF-AMS at 4 min time resolution. For the tracers described below, the mass concentration of chemical compositions e.g., sulfate, nitrate, and ion-speciated fragment were detected by HR-ToF-AMS, as shown in (Zhu et al., 2021b). The detail measurements of black carbon (BC) and nitrogen oxides (NOx) can also be found in Zhu et al., 2021b. In general, the ME-2 source analysis was performed by constraining two primary OA factors (the cooking POA, HOA) and two secondary OA factors (the cooking SOA, the vehicle LO-SOA) with the fixed a-value of 0.1 for HOA, 0.2 for cooking POA, 0.4 for vehicle LO-SOA and cooking SOA based on the same ambient OA datasets of the summer and winter observations in Shanghai. In ME-2 solutions from 1 to 7 factors, we found the solution of 6 factors (i.e., COA, HOA, Other-POA, Cooking SOA, Vehicle LO-SOA) was most interpretable for the wintertime observations. For the 5 factors solution, in addition to the constraint four factors, factor 5 appeared to be mixed primary and secondary features. However, Other-POA split into two factors with similar profiles in seven factors solution (**Fig.S13**). Source apportionment on OA datasets by using the unconstrained PMF model was also examined to compare with ME-2 analysis. The choice for the optimal solution for the PMF model was presented in the supporting information (**Fig.S14-S16** and **Table S19S20-S20S21**). Ambient PMF-resolved OA factors included POA factors (i.e., HOA, COA), and SOA factors i.e., OOA (oxygenated OA) in the winter observations in Shanghai, on average accounting for 27%, 35%, and 38% of OA mass. OOA resolved by PMF model did not separate

329 into two types of OOAs including LO-OOA and MO-OOA. Besides, we observed that HOA and COA profiles

330 (provided via PMF during the wintertime) contained high signals at the biomass burning tracer ion (m/z 73),

331 and m/z 91 (PAH-related m/z), indicating that the mixing among HOA, COA, and other ~~POA~~source emissions

332 (e.g., BBOA) (**Fig.5**).

333

334

335

336
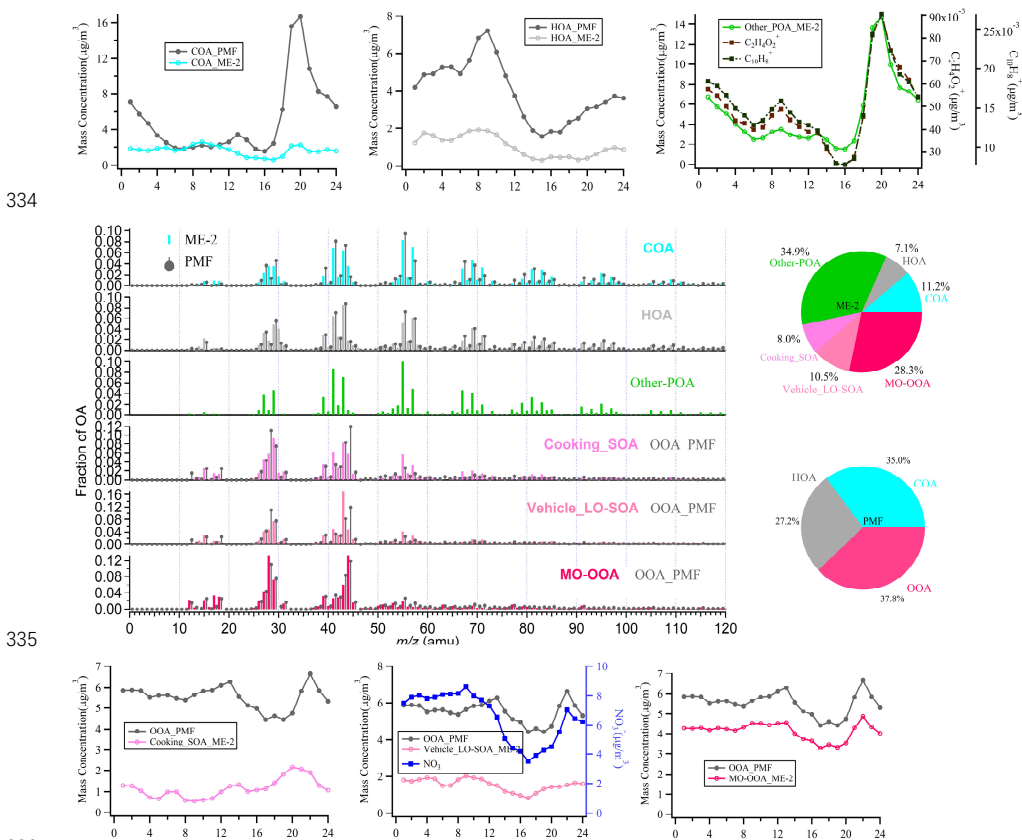
337 Fig.5. The comparison of the mass spectra, the diurnal variation, and fraction between ME-2 and PMF resolved factors during
338 the wintertime in Shanghai. The black lines in the spectra and diurnal pattern are the results of PMF analysis of the actual
339 atmosphere in Shanghai winter. The others correspond to the ME-2 source analysis results by using two primary OA factors
340 (the cooking POA, ambient HOA) and two secondary OA factors (the cooking SOA, the vehicle LO-SOA) as constraints
341 based on the same ambient OA datasets as the PMF model during the winter observations of Shanghai. Note that in the mass
342 spectra and daily patterns, the OOA_PMF factors which compared with vehicle LO-SOA and Cooking SOA respectively are
343 the same, rather than the two resolved factors.

344

As shown in **Fig.5**, compared with PMF results, the proportions of HOA (7%) and COA (11%) obtained by source apportionment with ME-2 have significantly decreased to the expected value during the winter observation(Huang et al., 2020; Xu et al., 2020). As expected, other POA contributions were identified in the highly polluted season, correlated well with $C_2H_4O_2^+$ and $C_{10}H_8^+$, which are well-known fragments from biomass burning and coal combustion emissions (**Fig.5**, **Fig.S17** and **Table S21S22**) (Alfarra et al., 2007; Duan et al., 2020; Hu et al., 2016a; Lee et al., 2010). The diurnal patterns of HOA_PMF were consistent with HOA_ME-2 during the winter observation, presenting low concentration during the daytime and high concentration at nighttime, likely due to the combined influence of boundary layer height and emissions from diesel vehicles during the nighttime. The temporal variation of two HOA factors showed a high correlation with NOx (Pearson r >0.7), suggesting two HOA factors are associated with vehicle emissions. Some variabilities existed between the diurnal cycle of COA_PMF and COA_ME-2. However, COA_ME-2 correlated better with $C_6H_{10}O^+$ than COA_PMF, which was considered a fragment tracer mainly from cooking emissions (Ge et al., 2012; Hu et al., 2016a; Sun et al., 2011; Xu et al., 2016). For SOA factors, the sum of cooking SOA and vehicle LO-SOA had a high correlation with nitrate (Pearson r = 0.84; **Fig.S17** and **Table S21S22**) and fragments of low-oxidizing substances ($C_2H_3O^+$; Pearson r = 0.95). In addition, we noticed that the vehicle SOA analyzed by ME-2 exhibited consistency with the diurnal variation of nitrate, especially the reasonable morning peak (~09:00) retained, implying that vehicle SOA is well separated by using ME-2 in winter. MO-OOA resolved via ME-2 was characterized by prominent signal at m/z 28 and m/z 44, consistent with those in OOA identified by using PMF and in other studies (Duan et al., 2020; Kim et al., 2017). Meanwhile, there was a strong correlation between MO-OOA time series and sulfate (Pearson r = 0.93), which was representative of regional aging species. Unfortunately, the SOA factor corresponding to other-POA (likely biomass burning OA) has not been resolved. Some studies have been found that OA emitted by biomass

367 burning will be rapidly oxidized in the ambient atmosphere, and the BBOA in the fresh plume is mostly aged

368 OA (Zhou et al., 2017). When the aged biomass burning OA is further oxidized, it is difficult to be identified

369 the biomass burning SOA from mixed within OOA without constraining its SOA factor. Overall, ME-2 source

370 analysis with the input of four source spectra profiles significantly improved the OA source apportionment

371 during the wintertime. In comparing the ME-2 analysis results with only two POA factors constraining to that

372 of the four factors constraining, the diurnal variations of HOA and COA obtained by constraining two primary

373 sources were more consistent with those of the ME-2 constraint four-factor than PMF. However, OOA and

374 POA were weakly separated, and the diurnal patterns of OOA were correlated with the case for the peak of

375 other-POA during the evening (20:00~21:00) (**Fig.S18-S19**). These phenomena imply that the SOA factor

376 constraint can be more environmentally meaningful factors to a certain extent.

377 For the source apportionment in summer with high oxidation conditions (**Fig.S20**), the fraction of COA

378 reduced from 21% (PMF result) to 12% (ME-2 result). Moreover, the diurnal patterns of ME-2 SOA factors

379 present more reasonable than PMF SOA factors. For example, the MO-OOA obtained based on ME-2 analysis

380 was in good agreement with the diurnal variation of O_x in summer. The Pearson r between MO-OOA_ME-2

381 and CO_2^+ (m/z 44), a marker of SOA was 0.95, higher than that of MO-OOA_PMF (0.79), which better reflects

382 the characteristics of the MO-OOA factor in ME-2 (**Fig.S21** and **Table** ~~S22~~**S23**). In general, the accurate

383 source apportionment results have significantly indicated that the reliability source profiles of the primary and

384 secondary of cooking and vehicles obtained in our study can be used as constraints for source apportionment

385 of OA with ME-2 in various primary emissions or high oxidation conditions.

386 4. **Limitations and future work**

387 POA emissions, and SOA formation in Go: PAM reactor from urban cooking and vehicular sources were

388 explored. The aged COA had higher hydrocarbon ions than aged HOA in mass spectra. The spectra profiles

389 of urban cooking and vehicular sources derived from the lab simulation were performed as constraints in ME-

2 model. The OA source apportionment using ME-2 compared with unconstrained PMF based on the HR OA datasets in Shanghai validated the reasonable of the primary and secondary source profiles of cooking and vehicles. It is noted that the vehicle experiments were solely conducted under a single engine with gasoline, and the cooking experiment only related to limited cooking styles. The variations of VOCs in diesel and gasoline vehicle emissions may lead to differences in the SOA characteristics (Wang et al., 2020). The POA and gas-phase precursor emitted from another cooking style - meat charbroiling can also form a large amount of SOA after photochemical oxidation (Kaltsonoudis et al., 2017). More work needs to be done to explore the POA and SOA mass spectrometric characteristics of emissions from vehicles and cooking sources. In addition, SOA mass spectra were split from aged COA and aged HOA by using the PMF model, and therefore provided limited information on dynamic SOA mass spectra; we suggested that further studies control the oxidation conditions to obtain a set of dynamic pure SOA spectral profile. Especially, the absence of primary HOA due to low emissions of engine, and the inability to separate vehicle PMF POA from aged HOA in the PMF analysis were major limitations of this study. In addition to obtaining pure vehicle POA through source experiments, further work can apply ME-2 model for constraining pure SOA profiles from experimental datasets to obtain the vehicle POA profiles. Constraining many SOA factors could be over-constraining the ME-2 runs, which leads to factor mixing and reduces the number of factors. Therefore, SOA source spectra can only be appropriately and reasonably limited in ME-2 model. Besides, measurements of accurate tracers for all factors that resolved by PMF or ME-2 model should be conducted in future work to improve source apportionment verification. For example, we had to combine vehicle LO-SOA and cooking SOA as LO-OOA due to the lack of the measurement tracers for vehicle and cooking SOA factor, and then we analyzed the time series-correlation of LO-OOA with nitrate and other tracer ions. Due to the limitation of Go: PAM, dilution and high concentration of OH radicals without other inorganic aerosol seeds were adopted to measure and simulate atmospheric aging of aerosols. Thus, the possible atmospheric transformations and the reaction pathway are

413   affected. In the future, it is still necessary to take further researches, for instance, use a quasi-atmospheric

414   aerosol evolution study (QUALITY) chamber (Guo et al., 2020) to study the SOA formation under different

415   actual oxidation conditions, like high/low NO_x and so forth. Moreover, ambient datasets obtained from

416   different sites and seasons need to be analyzed to validate the application of POA and SOA profiles of cooking

417   and vehicles in this study, noting selecting a loose constraint via a value in SOA factors due to their high

418   variability. Our research found that SOA from the urban cooking and vehicular sources contributed 19% and

419   35% of OA in the wintertime and summertime of Shanghai, implying the need to develop control measures to

420   reduce emissions from cooking and vehicular sources in the future.

421

422   **Nomenclature table**

Abbreviations	Description
OA	organic aerosol
POA	primary organic aerosol
SOA	secondary organic aerosol
HOA	hydrocarbon-like organic aerosol; associated with vehicle-related emissions in urban
COA	cooking organic aerosol
LO-OOA	low oxygenated organic aerosol
MO-OOA	more oxygenated organic aerosol
PMF	positive matrix factorization
ME-2	a multilinear engine
HR-ToF-AMS	high-resolution time-of-flight aerosol mass spectrometer
SMPS	scanning mobility particle sizers
Go: PAM	Gothenburg Potential Aerosol Mass reactor
VOCs	volatile organic compounds
SVOCs	semi-volatile organic compounds
IVOCs	intermediate volatile organic compounds
O-VOCs	oxygenated volatile organic compounds
$f_{28, 29, 41, 43…}$	fraction of m/z 28, 29, 41, 43… in total organic aerosol
aged HOA	organic aerosols oxidized by Potential Aerosol Mass reactor in vehicle experiments
aged COA	organic aerosols oxidized by Potential Aerosol Mass reactor in cooking experiments
LO-SOA	low oxidized vehicle secondary organic aerosol
MO-SOA	more oxidized vehicle secondary organic aerosol

Supporting information

Schematic depiction of the simulation and measurement system (Figure S1); Details of the mass spectra of aged HOA and aged COA (Figures S2-S5; Table ~~S4~~S5-~~S7~~S8); Van Krevelen diagram of POA, aged COA, and aged HOA (Figure S6); The choice for the PMF and ME-2 analysis (Figure S7-S10; Table ~~S8~~S9-~~S9~~S10; Figure S13-S14; Table ~~S19~~S20-~~S20~~S21); ME-2 source analysis during the summer observation in Shanghai (Figure S19); The time-series correlations of factors with external tracers (Figure S17-S18, S21; Table ~~S21~~S22-~~S22~~S23); Experimental parameters (Table S1-S3); Mass spectra similarity analysis between mass spectra of ambient factor and mass spectral profiles for vehicle and cooking (Table ~~S14~~S15-~~S18~~S19; Figure S11).

Data availability. The data provided in this paper can be obtained from the author upon request (songguo@pku.edu.cn).

域代码已更改

Author contribution. Wenfei Zhu, Zirui Zhang, Hui Wang, Ying Yu, Zheng Chen, Ruizhe Shen, Rui Tan, Kai Song, Kefan Liu, Rongzhi Tang, Yi Liu, Yuanju Li, Wenbin Zhang, and Zhou Zhang conducted the experiments. Wenfei Zhu, Zirui Zhang, Song Guo, and Min Hu analyzed the data. Shengrong Lou, Shijin Shuai, Hongming Xu, Shuangde Li, Yunfa Chen, Francesco Canonaco, and Andre. S. H. Prévôt reviewed and commented on the paper. Wenfei Zhu and Song Guo wrote the paper.

Competing interests. The authors declare no competing financial interest.

Acknowledgments. This research was supported by the National Natural Science Foundation of China (51636003, 41977179, 91844301), Beijing Municipal Science and Technology Commission (Z201100008220011), the Natural Science Foundation of Beijing (8192022), the fellowship of China Postdoctoral Science Foundation (2020M680242), and the Open Research Fund of State Key Laboratory of Multiphase Complex Systems (No. MPCS-2021-D-12).

References

446 Alfarra, M.R., Prevot, A.S.H., Szidat, S., Sandradewi, J., Weimer, S., Lanz, V.A., Schreiber, D., Mohr, M., Baltensperger, U., 2007.
447 Identification of the mass spectral signature of organic aerosols from wood burning emissions. Environmental Science &
448 Technology 41, 5770-5777.
449 Budisulistiorini, S.H., Canagaratna, M.R., Croteau, P.L., Marth, W.J., Baumann, K., Edgerton, E.S., Shaw, S.L., Knipping, E.M.,
450 Worsnop, D.R., Jayne, J.T., Gold, A., Surratt, J.D., 2013. Real-Time Continuous Characterization of Secondary Organic Aerosol
451 Derived from Isoprene Epoxydiols in Downtown Atlanta, Georgia, Using the Aerodyne Aerosol Chemical Speciation Monitor.
452 Environmental Science & Technology 47, 5686-5694.
453 Canagaratna, M., Jimenez, J., Kroll, J., Chen, Q., Kessler, S., Massoli, P., Hildebrandt Ruiz, L., Fortner, E., Williams, L., Wilson,
454 K., 2015. Elemental ration measurements of organic compounds using aerosol mass spectrometry: characterization,
455 improved calibration, and implications. Atmos. Chem. Phys 15, 253-272.
456 Canagaratna, M.R., Jayne, J.T., Jimenez, J.L., Allan, J.D., Alfarra, M.R., Zhang, Q., Onasch, T.B., Drewnick, F., Coe, H.,
457 Middlebrook, A., Delia, A., Williams, L.R., Trimborn, A.M., Northway, M.J., DeCarlo, P.F., Kolb, C.E., Davidovits, P., Worsnop,
458 D.R., 2007. Chemical and microphysical characterization of ambient aerosols with the aerodyne aerosol mass spectrometer.
459 Mass Spectrometry Reviews 26, 185-222.
460 Canonaco, F., Crippa, M., Slowik, J.G., Baltensperger, U., Prevot, A.S.H., 2013. SoFi, an IGOR-based interface for the efficient
461 use of the generalized multilinear engine (ME-2) for the source apportionment: ME-2 application to aerosol mass
462 spectrometer data. Atmospheric Measurement Techniques 6, 3649-3661.
463 Collier, S., Zhou, S., Kuwayama, T., Forestieri, S., Brady, J., Zhang, M., Kleeman, M., Cappa, C., Bertram, T., Zhang, Q., 2015.
464 Organic PM Emissions from Vehicles: Composition, O/C Ratio, and Dependence on PM Concentration. Aerosol Science and
465 Technology 49, 86-97.
466 Crippa, M., Canonaco, F., Lanz, V.A., Aijala, M., Allan, J.D., Carbone, S., Capes, G., Ceburnis, D., Dall'Osto, M., Day, D.A.,
467 DeCarlo, P.F., Ehn, M., Eriksson, A., Freney, E., Hildebrandt Ruiz, L., Hillamo, R., Jimenez, J.L., Junninen, H., Kiendler-Scharr,
468 A., Kortelainen, A.M., Kulmala, M., Laaksonen, A., Mensah, A., Mohr, C., Nemitz, E., O'Dowd, C., Ovadnevaite, J., Pandis, S.N.,
469 Petaja, T., Poulain, L., Saarikoski, S., Sellegri, K., Swietlicki, E., Tiitta, P., Worsnop, D.R., Baltensperger, U., Prevot, A.S.H., 2014.
470 Organic aerosol components derived from 25 AMS data sets across Europe using a consistent ME-2 based source
471 apportionment approach. Atmospheric Chemistry and Physics 14, 6159-6176.
472 Duan, J., Huang, R.-J., Li, Y., Chen, Q., Zheng, Y., Chen, Y., Lin, C., Ni, H., Wang, M., Ovadnevaite, J., Ceburnis, D., Chen, C.,
473 Worsnop, D.R., Hoffmann, T., O'Dowd, C., Cao, J., 2020. Summertime and wintertime atmospheric processes of secondary
474 aerosol in Beijing. Atmospheric Chemistry and Physics 20, 3793-3807.
475 Elser, M., Huang, R.-J., Wolf, R., Slowik, J.G., Wang, Q., Canonaco, F., Li, G., Bozzetti, C., Daellenbach, K.R., Huang, Y., Zhang,
476 R., Li, Z., Cao, J., Baltensperger, U., El-Haddad, I., Prevot, A.S.H., 2016. New insights into PM2.5 chemical composition and
477 sources in two major cities in China during extreme haze events using aerosol mass spectrometry. Atmospheric Chemistry
478 and Physics 16, 3207-3225.
479 Ge, X., Li, L., Chen, Y., Chen, H., Wu, D., Wang, J., Xie, X., Ge, S., Ye, Z., Xu, J., 2017. Aerosol characteristics and sources in
480 Yangzhou, China resolved by offline aerosol mass spectrometry and other techniques. Environmental Pollution 225, 74-85.
481 Ge, X., Setyan, A., Sun, Y., Zhang, Q., 2012. Primary and secondary organic aerosols in Fresno, California during wintertime:
482 Results from high resolution aerosol mass spectrometry. Journal of Geophysical Research-Atmospheres 117.
483 Gentner, D.R., Harley, R.A., Miller, A.M., Goldstein, A.H., 2009. Diurnal and Seasonal Variability of Gasoline-Related Volatile
484 Organic Compound Emissions in Riverside, California. Environmental Science & Technology 43, 4247-4252.
485 Guo, S., Hu, M., Guo, Q., Zhang, X., Zheng, M., Zheng, J., Chang, C.C., Schauer, J.J., Zhang, R., 2012. Primary Sources and
486 Secondary Formation of Organic Aerosols in Beijing, China. Environmental Science & Technology 46, 9846-9853.
487 Guo, S., Hu, M., Peng, J., Wu, Z., Zamora, M.L., Shang, D., Du, Z., Zheng, J., Fang, X., Tang, R., Wu, Y., Zeng, L., Shuai, S.,
488 Zhang, W., Wang, Y., Ji, Y., Li, Y., Zhang, A.L., Wang, W., Zhang, F., Zhao, J., Gong, X., Wang, C., Molina, M.J., Zhang, R., 2020.
489 Remarkable nucleation and growth of ultrafine particles from vehicular exhaust. Proceedings of the National Academy of
490 Sciences of the United States of America 117, 3427-3432.

491 Guo, S., Hu, M., Zamora, M.L., Peng, J., Shang, D., Zheng, J., Du, Z., Wu, Z., Shao, M., Zeng, L., Molina, M.J., Zhang, R., 2014.
492 Elucidating severe urban haze formation in China. Proceedings of the National Academy of Sciences of the United States of
493 America 111, 17373-17378.

494 He, L.Y., Huang, X.F., Xue, L., Hu, M., Lin, Y., Zheng, J., Zhang, R., Zhang, Y.H., 2011. Submicron aerosol analysis and organic
495 source apportionment in an urban atmosphere in Pearl River Delta of China using high-resolution aerosol mass
496 spectrometry. Journal of Geophysical Research Atmospheres 116, -.

497 He, L.Y., Lin, Y., Huang, X.F., Guo, S., Xue, L., Su, Q., Hu, M., Luan, S.J., Zhang, Y.H., 2010. Characterization of high-resolution
498 aerosol mass spectra of primary organic aerosol emissions from Chinese cooking and biomass burning. Atmospheric
499 Chemistry and Physics 10, 11535-11543.

500 Hu, W., Hu, M., Hu, W., Jimenez, J.L., Yuan, B., Chen, W., Wang, M., Wu, Y., Chen, C., Wang, Z., 2016a. Chemical composition,
501 sources, and aging process of submicron aerosols in Beijing: Contrast between summer and winter. Journal of Geophysical
502 Research Atmospheres 121, 1955-1977.

503 Hu, W., Hu, M., Hu, W.W., Zheng, J., Chen, C., Wu, Y., Guo, S., 2017. Seasonal variations in high time-resolved chemical
504 compositions, sources, and evolution of atmospheric submicron aerosols in the megacity Beijing. Atmospheric Chemistry &
505 Physics 17, 9979-10000.

506 Hu, W., Palm, B.B., Day, D.A., Campuzano-Jost, P., Krechmer, J.E., Peng, Z., de Sa, S.S., Martin, S.T., Alexander, M.L., Baumann,
507 K., Hacker, L., Kiendler-Scharr, A., Koss, A.R., de Gouw, J.A., Goldstein, A.H., Seco, R., Sjostedt, S.J., Park, J.-H., Guenther, A.B.,
508 Kim, S., Canonaco, F., Prevot, A.S.H., Brune, W.H., Jimenez, J.L., 2016b. Volatility and lifetime against OH heterogeneous
509 reaction of ambient isoprene-epoxydiols-derived secondary organic aerosol (IEPOX-SOA). Atmospheric Chemistry and
510 Physics 16, 11563-11580.

511 Huang, R.-J., He, Y., Duan, J., Li, Y., Chen, Q., Zheng, Y., Chen, Y., Hu, W., Lin, C., Ni, H., Dai, W., Cao, J., Wu, Y., Zhang, R., Xu,
512 W., Ovadnevaite, J., Ceburnis, D., Hoffmann, T., O'Dowd, C.D., 2020. Contrasting sources and processes of particulate species
513 in haze days with low and high relative humidity in wintertime Beijing. Atmospheric Chemistry and Physics 20, 9101-9114.

514 Huang, X.F., He, L.Y., Hu, M., Canagaratna, M.R., Kroll, J.H., Ng, N.L., Zhang, Y.H., Lin, Y., Xue, L., Sun, T.L., 2011.
515 Characterization of submicron aerosols at a rural site in Pearl River Delta of China using an Aerodyne High-Resolution
516 Aerosol Mass Spectrometer. Atmospheric Chemistry & Physics 11, 1865-1877.

517 Kaltsonoudis, C., Kostenidou, E., Louvaris, E., Psichoudaki, M., Tsiligiannis, E., Florou, K., Liangou, A., Pandis, S.N., 2017.
518 Characterization of fresh and aged organic aerosol emissions from meat charbroiling. Atmospheric Chemistry and Physics
519 17, 7143-7155.

520 Katragadda, H.R., Fullana, A., Sidhu, S., Carbonell-Barrachina, A.A., 2010. Emissions of volatile aldehydes from heated
521 cooking oils. Food Chemistry 120, 59-65.

522 Kim, H., Zhang, Q., Bae, G.-N., Kim, J.Y., Lee, S.B., 2017. Sources and atmospheric processing of winter aerosols in Seoul,
523 Korea: insights from real-time measurements using a high-resolution aerosol mass spectrometer. Atmospheric Chemistry
524 and Physics 17, 2009-2033.

525 Klein, F., Platt, S.M., Farren, N.J., Detournay, A., Bruns, E.A., Bozzetti, C., Daellenbach, K.R., Kilic, D., Kumar, N.K., Pieber, S.M.,
526 Slowik, J.G., Temime-Roussel, B., Marchand, N., Hamilton, J.F., Baltensperger, U., Prevot, A.S.H., El Haddad, I., 2016.
527 Characterization of Gas-Phase Organics Using Proton Transfer Reaction Time-of-Flight Mass Spectrometry: Cooking
528 Emissions. Environmental Science & Technology 50, 1243-1250.

529 Kostenidou, E., Lee, B.-H., Engelhart, G.J., Pierce, J.R., Pandis, S.N., 2009. Mass Spectra Deconvolution of Low, Medium, and
530 High Volatility Biogenic Secondary Organic Aerosol. Environmental Science & Technology 43, 4884-4889.

531 Kroll, J.H., Smith, J.D., Worsnop, D.R., Wilson, K.R., 2012. Characterisation of lightly oxidised organic aerosol formed from
532 the photochemical aging of diesel exhaust particles. Environmental Chemistry 9, 211-220.

533 Lee, T., Sullivan, A.P., Mack, L., Jimenez, J.L., Kreidenweis, S.M., Onasch, T.B., Worsnop, D.R., Malm, W., Wold, C.E., Hao, W.M.,
534 Collett, J.L., Jr., 2010. Chemical Smoke Marker Emissions During Flaming and Smoldering Phases of Laboratory Open Burning
535 of Wildland Fuels. Aerosol Science and Technology 44, I-V.

536 Li, J., Liu, Q., Li, Y., Liu, T., Huang, D., Zheng, J., Zhu, W., Hu, M., Wu, Y., Lou, S., Hallquist, A.M., Hallquist, M., Chan, C.K.,
537 Canonaco, F., Prevot, A.S.H., Fung, J.C.H., Lau, A.K.H., Yu, J.Z., 2019. Characterization of Aerosol Aging Potentials at Suburban
538 Sites in Northern and Southern China Utilizing a Potential Aerosol Mass (Go:PAM) Reactor and an Aerosol Mass
539 Spectrometer. Journal of Geophysical Research-Atmospheres 124, 5629-5649.
540 Li, Y.J., Sun, Y., Zhang, Q., Li, X., Li, M., Zhou, Z., Chan, C.K., 2017. Real-time chemical characterization of atmospheric
541 particulate matter in China: A review. Atmospheric Environment 158, 270-304.
542 Liu, T., Li, Z., Chan, M., Chan, C.K., 2017. Formation of secondary organic aerosols from gas-phase emissions of heated
543 cooking oils. Atmospheric Chemistry and Physics 17, 7333-7344.
544 Liu, T., Wang, Z., Wang, X., Chan, C.K., 2018. Primary and secondary organic aerosol from heated cooking oil emissions.
545 Atmospheric Chemistry and Physics 18, 11363-11374.
546 Louvaris, E.E., Karnezi, E., Kostenidou, E., Kaltsonoudis, C., Pandis, S.N., 2017. Estimation of the volatility distribution of
547 organic aerosol combining thermodenuder and isothermal dilution measurements. Atmospheric Measurement Techniques
548 10, 3909-3918.
549 Mohr, C., DeCarlo, P.F., Heringa, M.F., Chirico, R., Slowik, J.G., Richter, R., Reche, C., Alastuey, A., Querol, X., Seco, R., Penuelas,
550 J., Jimenez, J.L., Crippa, M., Zimmermann, R., Baltensperger, U., Prevot, A.S.H., 2012. Identification and quantification of
551 organic aerosol from cooking and other sources in Barcelona using aerosol mass spectrometer data. Atmospheric Chemistry
552 and Physics 12, 1649-1665.
553 Ng, N.L., Canagaratna, M.R., Jimenez, J.L., Zhang, Q., Ulbrich, I.M., Worsnop, D.R., 2011. Real-Time Methods for Estimating
554 Organic Component Mass Concentrations from Aerosol Mass Spectrometer Data. Environmental Science & Technology 45,
555 910-916.
556 Paatero, P., 1999. The multilinear engine - A table-driven, least squares program for solving multilinear problems, including
557 the n-way parallel factor analysis model. Journal of Computational and Graphical Statistics 8, 854-888.
558 Paatero, P., Hopke, P.K., 2003. Discarding or downweighting high-noise variables in factor analytic models. Analytica
559 Chimica Acta 490, 277-289.
560 Peng, Z., Day, D.A., Ortega, A.M., Palm, B.B., Hu, W., Stark, H., Li, R., Tsigaridis, K., Brune, W.H., Jimenez, J.L., 2016. Non-OH
561 chemistry in oxidation flow reactors for the study of atmospheric chemistry systematically examined by modeling.
562 Atmospheric Chemistry and Physics 16, 4283-4305.
563 Presto, A.A., Gordon, T.D., Robinson, A.L., 2014. Primary to secondary organic aerosol: evolution of organic emissions from
564 mobile combustion sources. Atmospheric Chemistry and Physics 14, 5015-5036.
565 Qin, Y.M., Tan, H.B., Li, Y.J., Schurman, M.I., Li, F., Canonaco, F., Prevot, A.S.H., Chan, C.K., 2017. Impacts of traffic emissions
566 on atmospheric particulate nitrate and organics at a downwind site on the periphery of Guangzhou, China. Atmospheric
567 Chemistry and Physics 17, 10245-10258.
568 Reyes-Villegas, E., Green, D.C., Priestman, M., Canonaco, F., Coe, H., Prevot, A.S.H., Allan, J.D., 2016. Organic aerosol source
569 apportionment in London 2013 with ME-2: exploring the solution space with annual and seasonal analysis. Atmospheric
570 Chemistry and Physics 16, 15545-15559.
571 Robinson, A.L., Donahue, N.M., Shrivastava, M.K., Weitkamp, E.A., Sage, A.M., Grieshop, A.P., Lane, T.E., Pierce, J.R., Pandis,
572 S.N., 2007. Rethinking organic aerosols: Semivolatile emissions and photochemical aging. Science 315, 1259-1262.
573 Schauer, J.J., Kleeman, M.J., Cass, G.R., Simoneit, B.R.T., 2002. Measurement of emissions from air pollution sources. 4. C-1-
574 C-27 organic compounds from cooking with seed oils. Environmental Science & Technology 36, 567-575.
575 Sun, J., Zhang, Q., Canagaratna, M.R., Zhang, Y., Ng, N.L., Sun, Y., Jayne, J.T., Zhang, X., Zhang, X., Worsnop, D.R., 2010.
576 Highly time-and size-resolved characterization of submicron aerosol particles in Beijing using an Aerodyne Aerosol Mass
577 Spectrometer. Atmospheric Environment 44, 131-140.
578 Sun, Y., Du, W., Fu, P., Wang, Q., Li, J., Ge, X., Zhang, Q., Zhu, C., Ren, L., Xu, W., 2016. Primary and secondary aerosols in
579 Beijing in winter: sources, variations and processes. Atmospheric Chemistry & Physics 16, 1-41.
580 Sun, Y., Jiang, Q., Wang, Z., Fu, P., Li, J., Yang, T., Yin, Y., 2014. Investigation of the sources and evolution processes of severe
581 haze pollution in Beijing in January 2013. Journal of Geophysical Research Atmospheres 119, 4380-4398.

582   Sun, Y., Xu, W., Zhang, Q., Jiang, Q., Canonaco, F., Prévôt, A.S., Fu, P., Li, J., Jayne, J., Worsnop, D.R., 2018. Source
583   apportionment of organic aerosol from two-year highly time-resolved measurements by an aerosol chemical speciation
584   monitor in Beijing, China. Atmospheric Chemistry and Physics Discussions, 1-33.
585   Sun, Y.L., Zhang, Q., Schwab, J.J., Demerjian, K.L., Chen, W.N., Bae, M.S., Hung, H.M., Hogrefe, O., Frank, B., Rattigan, O.V.,
586   Lin, Y.C., 2011. Characterization of the sources and processes of organic and inorganic aerosols in New York city with a
587   high-resolution time-of-flight aerosol mass apectrometer. Atmospheric Chemistry and Physics 11, 1581-1602.
588   Tang, R.Z., Lu, Q.Y., Guo, S., Wang, H., Song, K., Yu, Y., Tan, R., Liu, K.F., Shen, R.Z., Chen, S.Y., Zeng, L.M., Jorga, S.D., Zhang,
589   Z., Zhang, W.B., Shuai, S.J., Robinson, A.L., 2021. Measurement report: Distinct emissions and volatility distribution of
590   intermediate-volatility organic compounds from on-road Chinese gasoline vehicles: implication of high secondary organic
591   aerosol formation potential. Atmospheric Chemistry and Physics 21, 2569-2583.
592   Ulbrich, I., Canagaratna, M., Zhang, Q., Worsnop, D., Jimenez, J., 2009. Interpretation of organic components from positive
593   matrix factorization of aerosol mass spectrometric data. Atmospheric Chemistry & Physics 9.
594   Wang, H., Guo, S., Yu, Y., Shen, R., Zhu, W., Tang, R., Tan, R., Liu, K., Song, K., Zhang, W., Zhang, Z., Shuai, S., Xu, H., Zheng,
595   J., Chen, S., Li, S., Zeng, L., Wu, Z., 2021. Secondary aerosol formation from a Chinese gasoline vehicle: Impacts of fuel (E10,
596   gasoline) and driving conditions (idling, cruising). The Science of the total environment 795, 148809-148809.
597   Wang, H., Xiang, Z., Wang, L., Jing, S., Lou, S., Tao, S., Liu, J., Yu, M., Li, L., Lin, L., Chen, Y., Wiedensohler, A., Chen, C., 2018.
598   Emissions of volatile organic compounds (VOCs) from cooking and their speciation: A case study for Shanghai with
599   implications for China. Science of the Total Environment 621, 1300-1309.
600   Wang, J., Ge, X., Chen, Y., Shen, Y., Zhang, Q., Sun, Y., Xu, J., Ge, S., Yu, H., Chen, M., 2016. Highly time-resolved urban
601   aerosol characteristics during springtime in Yangtze River Delta, China: insights from soot particle aerosol mass spectrometry.
602   Atmospheric Chemistry and Physics 16, 9109-9127.
603   Wang, M., Li, S., Zhu, R., Zhang, R., Zu, L., Wang, Y., Bao, X., 2020. On-road tailpipe emission characteristics and ozone
604   formation potentials of VOCs from gasoline, diesel and liquefied petroleum gas fueled vehicles. Atmospheric Environment
605   223.
606   Wang, Y.C., Huang, R.J., Ni, H.Y., Chen, Y., Wang, Q.Y., Li, G.H., Tie, X.X., Shen, Z.X., Huang, Y., Liu, S.X., Dong, W.M., Xue, P.,
607   Frohlich, R., Canonaco, F., Elser, M., Daellenbach, K.R., Bozzetti, C., Haddad, I.E., Prevot, A.S.H., Canagaratna, M.R., Worsnop,
608   D.R., Cao, J.J., 2017. Chemical composition, sources and secondary processes of aerosols in Baoji city of northwest China.
609   Atmospheric Environment 158, 128-137.
610   Watne, A.K., Psichoudaki, M., Ljungstrom, E., Le Breton, M., Hallquist, M., Jerksjo, M., Fallgren, H., Jutterstrom, S., Hallquist,
611   A.M., 2018. Fresh and Oxidized Emissions from In-Use Transit Buses Running on Diesel, Biodiesel, and CNG. Environmental
612   Science & Technology 52, 7720-7728.
613   Xu, J., Shi, J., Zhang, Q., Ge, X., Canonaco, F., Prévôt, A.S., Vonwiller, M., Szidat, S., Ge, J., Ma, J., 2016. Wintertime organic
614   and inorganic aerosols in Lanzhou, China: sources, processes, and comparison with the results during summer. Atmospheric
615   Chemistry and Physics 16, 14937-14957.
616   Xu, W., Han, T., Wei, D., Wang, Q., Chen, C., Jian, Z., Zhang, Y., Jie, L., Fu, P., Wang, Z., 2017. Effects of Aqueous-phase and
617   Photochemical Processing on Secondary Organic Aerosol Formation and Evolution in Beijing, China. Environmental Science
618   & Technology 51, 762.
619   Xu, W., He, Y., Qiu, Y., Chen, C., Xie, C., Lei, L., Li, Z., Sun, J., Li, J., Fu, P., Wang, Z., Worsnop, D., Sun, Y., 2020. Mass spectral
620   characterization of primary emissions and implications in source apportionment of organic aerosol. Atmospheric
621   Measurement Techniques 13, 3205-3219.
622   Ying, Y.A.B., Hui, W.A., A, T.W., Kai, S.A., A, T.T., A, Z.W., C, Y.G., A, H.D., A, S.C., D, L.Z.A.B., 2020. Elucidating the importance
623   of semi-volatile organic compounds to secondary organic aerosol formation at a regional site during the EXPLORE-YRD
624   campaign - ScienceDirect. Atmospheric Environment.
625   Yu, Y., Wang, H., Wang, T.T., Song, K., Tan, T.Y., Wan, Z.C., Gao, Y.Q., Dong, H.B., Chen, S.Y., Zeng, L.M., Hu, M., Wang, H.L.,
626   Lou, S.R., Zhu, W.F., Guo, S., 2021. Elucidating the importance of semi-volatile organic compounds to secondary organic
627   aerosol formation at a regional site during the EXPLORE-YRD campaign. Atmospheric Environment 246.

628 Zhang, Q., Jimenez, J.L., Canagaratna, M.R., Ulbrich, I.M., Ng, N.L., Worsnop, D.R., Sun, Y., 2011. Understanding atmospheric
629 organic aerosols via factor analysis of aerosol mass spectrometry: a review. Analytical & Bioanalytical Chemistry 401, 3045-
630 3067.
631 Zhang, X., Zhang, Y., Sun, J., Yu, Y., Canonaco, F., Prevot, A.S.H., Li, G., 2017a. Chemical characterization of submicron aerosol
632 particles during wintertime in a northwest city of China using an Aerodyne aerosol mass spectrometry. Environmental
633 Pollution 222, 567-582.
634 Zhang, Y., Tang, L., Sun, Y., Favez, O., Canonaco, F., Albinet, A., Couvidat, F., Liu, D., Jayne, J.T., Wang, Z., Croteau, P.L.,
635 Canagaratna, M.R., Zhou, H.-c., Prevot, A.S.H., Worsnop, D.R., 2017b. Limited formation of isoprene epoxydiols-derived
636 secondary organic aerosol under NOx-rich environments in Eastern China. Geophysical Research Letters 44, 2035-2043.
637 Zhang, Y.J., Tang, L.L., Wang, Z., Yu, H.X., Sun, Y.L., Liu, D., Qin, W., Zhang, H.L., Zhou, H.C., 2014. Insights into characteristics,
638 sources and evolution of submicron aerosols during harvest seasons in Yangtze River Delta (YRD) region, China.
639 Atmospheric Chemistry & Physics 14, 9109-9154.
640 Zhang, Z., Zhu, W., Hu, M., Wang, H., Chen, Z., Shen, R., Yu, Y., Tan, R., Guo, S., 2020. Secondary Organic Aerosol from
641 Typical Chinese Domestic Cooking Emissions. Environmental Science & Technology Letters.
642 Zhou, S., Collier, S., Jaffe, D.A., Briggs, N.L., Hee, J., Sedlacek, A.J., III, Kleinman, L., Onasch, T.B., Zhang, Q., 2017. Regional
643 influence of wildfires on aerosol chemistry in the western US and insights into atmospheric aging of biomass burning organic
644 aerosol. Atmospheric Chemistry and Physics 17, 2477-2493.
645 Zhou, W., Wang, Q., Zhao, X., Xu, W., Chen, C., Du, W., Zhao, J., Canonaco, F., Prevot, A.S.H., Fu, P., Wang, Z., Worsnop, D.R.,
646 Sun, Y., 2018. Characterization and source apportionment of organic aerosol at 260 m on a meteorological tower in Beijing,
647 China. Atmospheric Chemistry and Physics 18, 3951-3968.
648 Zhu, Q., Huang, X.-F., Cao, L.-M., Wei, L.-T., Zhang, B., He, L.-Y., Elser, M., Canonaco, F., Slowik, J.G., Bozzetti, C., El-Haddad,
649 I., Prevot, A.S.H., 2018. Improved source apportionment of organic aerosols in complex urban air pollution using the
650 multilinear engine (ME-2). Atmospheric Measurement Techniques 11, 1049-1060.
651 Zhu, W., Guo, S., Lou, S., Wang, H., Yu, Y., Xu, W., Liu, Y., Cheng, Z., Huang, X., He, L., Zeng, L., Chen, S., Hu, M., 2021a. A
652 novel algorithm to determine the scattering coefficient of ambient organic aerosols. Environmental Pollution 270.
653 Zhu, W., Zhou, M., Cheng, Z., Yan, N., Huang, C., Qiao, L., Wang, H., Liu, Y., Lou, S., Guo, S., 2021b. Seasonal variation of
654 aerosol compositions in Shanghai, China: Insights from particle aerosol mass spectrometer observations. The Science of the
655 total environment 771, 144948-144948.

656